UC Irvine
UC Irvine Previously Published Works

Title

LMODEL: A Satellite Precipitation Methodology Using Cloud Development Modeling. Part II: Validation

Permalink

https://escholarship.org/uc/item/8cd3503f

Authors

Hsu, Kuo-lin
Bellerby, Tim
Sorooshian, S

LMODEL: A Satellite Precipitation Methodology Using Cloud Development Modeling. Part II: Validation

KUO-LIN HSU

University of California, Irvine, Irvine, California

TIM BELLERBY

University of Hull, Hull, United Kingdom

S. SOROOSHIAN

University of California, Irvine, Irvine, California

ABSTRACT

A new satellite-based rainfall monitoring algorithm that integrates the strengths of both low Earth-orbiting (LEO) and geostationary Earth-orbiting (GEO) satellite information has been developed. The Lagrangian Model (LMODEL) algorithm combines a 2D cloud-advection tracking system and a GEO data–driven cloud development and rainfall generation model with procedures to update model parameters and state variables in near–real time. The details of the LMODEL algorithm were presented in Part I. This paper describes a comparative validation against ground radar rainfall measurements of 1- and 3-h LMODEL accumulated rainfall outputs. LMODEL rainfall estimates consistently outperform accumulated 3-h microwave (MW)-only rainfall estimates, even before the more restricted spatial coverage provided by the latter is taken into account. In addition, the performance of LMODEL products remains effective and consistent between MW overpasses. Case studies demonstrate that the LMODEL provides the potential to synergize available satellite data to generate useful precipitation measurements at an hourly scale.

1. Introduction

Floods caused by extreme precipitation events are among the most serious natural disasters worldwide. A recent Intergovernmental Panel on Climate Change report concludes that global warming will have a direct effect on the frequency of extreme precipitation events (Solomon et al. 2007). They also suggest that future tropical cyclones will become more intense, with higher peak wind speeds and heavier precipitation. The International Strategy for Disaster Reduction (ISDR) program of the United Nations reports that 8 out of the top 10 most deadly natural disasters in 2007 were flood related (ISDR 2008). Floods also surpass other types of natural disaster—such as droughts, earthquakes, and wild fires—in terms of their scale of impact. In 2007, flood events triggered by the extreme precipitation adversely affected the life and property of more than 160 million people. On 2 May 2008, Cyclone Nargis generated heavy rainfall that led to flooding and landslides, causing catastrophic destruction and at least 130 000 reported fatalities. Moreover, Hurricane Katrina's effect on New Orleans in 2005 shows that the developed countries are not immune from such disasters (Martine and Marshall 2007). Clearly, accurate monitoring of extreme precipitation is a key element for improving operational weather forecasts and for implementing flood forecasting systems. Unfortunately, many parts of the world have limited or nonexisting monitoring systems capable of predicting flooding from extreme rainfall. Traditional precipitation observations using synoptic rain gauges are limited to point measurements, and precipitation observations from radar sensors are limited by considerable blockage over mountainous watersheds in addition to high capital costs beyond the reach of many nations. Therefore, continuing improvement of high-resolution satellite-based methodologies to

Corresponding author address: T. J. Bellerby, Department of Geography, University of Hull, Hull HU6 7RX, United Kingdom. E-mail: t.j.bellerby@hull.ac.uk

provide reliable estimates of the quantity and distribution of precipitation is critical to a wide range of hydrological and hydrometeorological applications.

Recent developments in satellite remote sensing techniques provide a unique opportunity for consistent precipitation observation at a global scale. However, the task of obtaining precipitation measurements from satellites still faces significant challenges in terms of reconciling heterogeneities in sensor capabilities and associated platform orbits. Geostationary Earth-orbiting (GEO) satellites are capable of providing images every 15–30 min in multiple spectral bands, but their spectral coverage is limited to visible and infrared wave bands that resolve cloud patterns rather than the hydrometeors directly relevant to surface rainfall rates. Therefore, as reported in numerous studies, GEO infrared (IR)–based rainfall algorithms are most effective at identifying tropical convective systems whose cold high tops show prominently in GEO-IR imagery and perform less well in the presence of warm low-lying clouds and cold high cirrus clouds (Arkin and Meisner 1987; Adler and Negri 1988). Some improvement may be gained by employing cloud classification approaches using texture measures and cloud-patch identification and additional improvements made by combining information from multispectral imagery (Ba and Gruber 2001; Bellerby et al. 2000; Bellerby 2004; Capacci and Conway 2005; Hong et al. 2004; Turk and Miller 2005). However, the most significant improvements in precipitation retrieval have been achieved by locally adjusting GEO-IR retrievals using near-real-time low Earth-orbiting (LEO) microwave (MW)-based rainfall estimation or other collateral data (Ba and Gruber 2001; Bellerby et al. 2000; Bellerby 2004; Hsu et al. 1997; Huffman et al. 2007; Kidd et al. 2003; Marzano et al. 2004; Nicholson et al. 2003a, 2003b; Sorooshian et al. 2000; Todd et al. 2001; Turk and Miller 2005; Vicente et al. 1998; Xu et al. 1999).

MW sensors on LEO satellites provide more direct information on the hydrometeor distribution in rain clouds than GEO imagery. However, the low sampling frequency of LEO satellites limits the effectiveness of MW rainfall retrieval at short time scales. By integrating multiple LEO satellite information, considerable improvement in short-time-scale rainfall retrieval has been achieved (Huffman et al. 2007). In addition, the Tropical Rainfall Measurement Mission (TRMM) launched in 1997 carried the first orbital rainfall radar. This may be used to calibrate passive microwave sensors on other spacecraft, resulting in significant improvements to rainfall retrievals over the tropics (Kummerow et al. 1998, 2000; Simpson et al. 1988). The follow-up mission to TRMM, the Global Precipitation Measurement (GPM) mission planned for launch in 2013, will deploy an enhanced dual-frequency radar sensor. The GPM program aims to combine observations from multiple passive microwave sensors mounted on both preexisting and newly deployed satellites. The planned GPM satellite constellation will be able to sample more than 90% of the globe with a return interval of three hours or less (Hou et al. 2008). Such intensive sampling of precipitation will provide unprecedented information of the global water and energy distributions at fine time scales.

Although the combined LEO sampling frequency in the GPM era is planned to reach a near 3-h return interval, instantaneous sampling by MW satellite sensor overpasses does not provide a complete solution for monitoring accumulated rainfall at high temporal resolutions. Heavy precipitation generated from convective cloud systems (CCSs) may develop over a significantly shorter period than this, resulting in sampling errors in the corresponding 3-h estimated rainfall totals. Some CCSs are short-life events, which may not coincide with MW overpasses; however, other CCSs may generate high rainfall intensities over a very short duration but not be sampled by the MW sensors. In both of these cases, accumulated LEO rainfall retrievals will suffer from a negative bias. Overestimates are also possible, when short-duration bursts of high-intensity rainfall coincide with a MW overpass and are assumed to be typical of an entire 3-h period. It must also be noted that the combined temporal sampling frequency provided by LEO satellites has varied significantly with time, and a study of currently planned satellite missions suggests that this variation is likely to continue. Sampling capability is likely to peak during the GPM era and then fall back to a lower relative value. This variation poses significant challenges to the satellite rainfall community: both in terms of providing reliable operational precipitation measurements and in generating a consistent long-term database for hydrometeorological and hydroclimatological studies. In light of these difficulties, the continuing development of effective retrieval algorithms capable of integrating multiple sensors and platforms with flexible and efficient modern data assimilation (DA) techniques is essential.

Recent work has demonstrated the effectiveness of using GEO-derived cloud motion vectors to "morph" MW rainfall estimates between sensor overpasses. The original Climate Prediction Center (CPC) morphing (CMORPH) algorithm applied an empirical correction to compensate for the difference between average cloud advection and the motion of surface rainfall and then linearly interpolated MW rainfall estimates along advection streamlines (Joyce et al. 2004). This approach alleviates some of the difficulties mentioned earlier, but it cannot fully compensate for sampling issues associated with short-lived storms. The CMORPH concept has been

refined using data assimilation (Kalman filter) approaches to update the advected rainfall values by comparing them to simple rainfall estimates derived from GEO imagery (Okamoto et al. 2005). Data assimilation approaches are very attractive in this context because they can take into account the considerable uncertainty in the GEO rainfall estimates when updating the advected values. They also fulfill the requirement for near-real-time estimates imposed by many operational applications. In a parallel development, a number of studies have reported significant relationships between developing cloud cells in GEO imagery and evolving rainstorms (Machado et al. 1998; Horsfield 2006). These developments suggest the possibility of running a simple storm development model between MW overpasses rather than interpolating or updating MW rainfall estimates directly. Such an approach would use the relationship between changes in cloud patterns and changes in rainfall processes rather than attempt to determine a static relationship between GEO cloud imagery and rainfall, and it would use DA techniques to update model representations of rainfall processes rather than attempt to adjust the rainfall values themselves.

A new multiplatform multisensor satellite rainfall algorithm has been developed to evaluate the effectiveness of the cloud development modeling/model updating approach. The Lagrangian Model (LMODEL) methodology synergizes recent developments in cloud development modeling, satellite cloud-feature extraction, cloud image tracking, geostatistics, and sequential filtering theory to develop a combined IR/microwave algorithm for rainfall retrieval. Part I of this paper (Bellerby et al. 2009) describes the algorithm in detail. This paper presents a validation of LMODEL outputs and evaluates the performance of the new algorithm.

2. Methodology

a. LMODEL algorithm

LMODEL is an integrated rainfall estimation algorithm developed to combine the strengths of LEO and GEO satellite data from current and future satellite missions (e.g., GPM) by making optimal use of the complementary nature of different sensors and their respective sampling capabilities. The algorithm consists of 1) a high-resolution 2D cloud tracking system, which captures cloud advection from successive GEO satellite images; 2) a cloud development and rainfall-generation model; and 3) local updating of model fluxes and state variables against MW rainfall data.

The cloud development model is a semi-Lagrangian cloud precipitable water balance model. Convective and
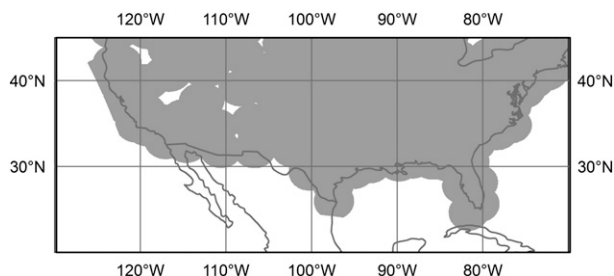

FIG. 1. Study area and radar coverage.

stratiform precipitable water inputs are estimated from brightness temperatures and brightness temperature changes in infrared geostationary satellite imagery. This imagery is also used to quantify cloud dispersal. These forcing factors modify the cloud precipitable water as it is tracked along cloud-advection streamlines using the very high-resolution cloud tracking algorithm of Bellerby (2006). The model operates at full geostationary pixel resolution, but it is designed to provide products at spatial and temporal resolutions somewhat lower than this resolution.

Model updating takes place in two stages. The first stage determines a local scaling parameter by comparing unmodified model outputs against rainfall estimates from coincident MW overpasses and kriging the resulting anomalies along advection streamlines. The interpolated parameter is used to scale precipitable water fluxes into the model. The second stage uses a Kalman filter to update model states.

b. Dataset

The study area used for model development and testing is the conterminous United States (CONUS) covering 20°–45°N and 70°–130°W (see Fig. 1) for two periods: July–August 2006 and February–March 2007. The LMODEL algorithm requires several data sources from GEO and LEO satellites for model development and estimation. One dataset used is the full-resolution global GEO-IR data at every half-hour at 0.04° resolution, provided by the Climate Prediction Center of the National Oceanic and Atmospheric Administration (NOAA; Janowiak et al. 2001). This dataset is a composite of infrared (~11 μm) imagery from the multifunctional transport satellite [MTSAT; formerly the geostationary meteorological satellite (GMS)], Geostationary Operational Environmental Satellite (GOES), and Meteosat satellites with zenith angle corrections used to match brightness temperatures away from the respective subsatellite points. Microwave rainfall estimates were obtained from the CPC Merged Microwave Dataset (CPC 2008), which composites estimates from multiple LEO satellites and sensors, including the Defense Meteorological Satellite Program Special

TABLE 1. Validation of 3-h LMODEL rainfall products against ground radar at a range of spatial resolutions. Stage 1 products are outputs from the unadjusted model. Stage 2 products rescale local precipitable water fluxes. Stage 3 products incorporate both local flux scaling and Kalman filter state adjustment.

Resolution	Correlation (r)			RMSE (mm h^{-1})			Bias (mm h^{-1})			Skill (%)		
	1	2	3	1	2	3	1	2	3	1	2	3
June 2006												
0.04°	0.461	0.520	0.544	0.887	0.855	0.840	−0.062	−0.058	−0.55	91.9	92.3	92.8
0.24°	0.519	0.588	0.618	0.770	0.732	0.714	−0.063	−0.059	−0.55	91.9	92.4	92.9
0.48°	0.555	0.628	0.660	0.692	0.653	0.633	−0.063	−0.059	−0.55	91.6	92.3	92.8
1.00°	0.613	0.684	0.714	0.567	0.531	0.511	−0.063	−0.059	−0.55	91.4	92.1	92.7
July 2006												
0.04°	0.441	0.522	0.543	0.863	0.823	0.812	−0.058	−0.052	−0.051	91.3	91.7	92.2
0.24°	0.515	0.613	0.643	0.702	0.653	0.637	−0.058	−0.052	−0.051	91.1	91.6	92.2
0.48°	0.559	0.665	0.697	0.609	0.557	0.540	−0.058	−0.052	−0.050	91.0	91.5	92.1
1.00°	0.607	0.719	0.753	0.502	0.541	0.433	−0.058	−0.052	−0.051	90.7	91.6	92.1
August 2006												
0.04°	0.479	0.523	0.546	0.837	0.809	0.797	−0.062	−0.055	−0.055	91.2	91.5	92.0
0.24°	0.564	0.619	0.649	0.674	0.637	0.622	−0.062	−0.055	−0.055	90.9	91.2	91.7
0.48°	0.616	0.673	0.707	0.579	0.539	0.522	−0.062	−0.055	−0.055	90.6	91.1	91.6
1.00°	0.679	0.733	0.768	0.463	0.426	0.409	−0.061	−0.055	−0.054	90.3	91.0	91.4
February 2007												
0.04°	0.379	0.427	0.461	0.439	0.429	0.420	−0.010	−0.010	−0.007	91.2	91.5	97.7
0.24°	0.421	0.472	0.511	0.407	0.395	0.386	−0.012	−0.013	−0.010	91.4	91.7	92.0
0.48°	0.450	0.503	0.542	0.382	0.370	0.360	−0.013	−0.014	−0.011	91.2	91.6	92.0
1.00°	0.496	0.546	0.584	0.338	0.326	0.317	−0.014	−0.015	−0.012	90.9	91.4	91.8
March 2007												
0.04°	0.478	0.528	0.561	0.510	0.493	0.481	−0.014	−0.014	−0.011	91.4	91.8	92.2
0.24°	0.523	0.577	0.645	0.465	0.445	0.431	−0.016	−0.015	−0.013	91.5	91.9	92.5
0.48°	0.556	0.611	0.651	0.427	0.407	0.391	−0.017	−0.016	−0.014	91.4	91.9	92.5
1.00°	0.608	0.662	0.703	0.365	0.343	0.327	−0.017	−0.017	−0.015	91.3	91.9	92.6

Sensor Microwave Imager (DMSP SSM/I), the Polar Orbiting Environmental Satellite Advanced Microwave Sounding Unit B (POES AMSU-B), the *Aqua* Advanced Microwave Scanning Radiometer for Earth Observing System (AMSR-E), and the TRMM Microwave Imager (TMI). Instantaneous rainfall estimates are generated from the just-mentioned sensors and platforms using separate algorithms over the land and ocean and interpolated to a common 0.08° spatial resolution (Ferraro et al. 2000; Kummerow et al. 2001; Weng et al. 2003). The CPC MW rainfall data were further interpolated to a 0.04° spatial resolution by mapping the center of each 0.08° pixel onto a single 0.04° pixel and then interpolating those high-resolution pixels with values defined for at least two immediate neighbors. This preprocessing step helped to remove some missing data pixels from the middle of swaths. The interpolated MW data were then collocated to the GEO clouds using the algorithm described in Bellerby et al. (2009).

LMODEL algorithm performance was evaluated against the combined rainfall observations from ground-based weather radar systems, provided by the NOAA National Centers for Environmental Prediction (NCEP) and Environmental Modeling Center (EMC) (Lin and Mitchell 2005). The NCEP/EMC 4-km gridded radar rainfall estimates were remapped to a 0.04° latitude–longitude grid compatible with LMODEL estimates. The available radar coverage is shown in Fig. 1.

The summer-season rainfall may be expected to be dominated by convective processes, with the North American monsoon bringing moisture to the southwestern states (Adams and Comrie 1997) and mesoscale convective complexes developing across the Great Plains (Ashley et al. 2003). Winter-season rainfall is more likely to be characterized by frontal systems associated with extratropical cyclones, particularly in the northern states and mountainous regions (Court 1974). Winter precipitation contains significant snowfall in many regions, causing problems with MW rainfall retrievals, which leads to data voids (Ferraro et al. 2000).

c. Collocation of microwave data to GEO cloud imagery

An empirical collocation procedure, described in detail in Bellerby et al. (2009), is used to move the MW rainfall to the IR clouds, compensating for the combined effects of measurement timing differences, geolocation error, parallax, and shear. The MW data are initially interpolated to GEO-IR pixel resolution and then the collocation algorithm processes each pixel location. Two

TABLE 2. Same as Table 1 but for 1-h LMODEL rainfall products.

Resolution	Correlation (r)			RMSE (mm h^{-1})			Bias (mm h^{-1})			Skill (%)		
	1	2	3	1	2	3	1	2	3	1	2	3
June 2006												
0.04°	0.389	0.438	0.453	1.070	1.041	1.030	−0.062	−0.058	−0.055	92.8	93.0	93.5
0.24°	0.459	0.520	0.542	0.900	0.863	0.847	−0.063	−0.058	−0.055	92.4	92.7	93.2
0.48°	0.506	0.573	0.597	0.787	0.747	0.729	−0.063	−0.058	−0.055	92.0	92.4	92.9
1.00°	0.577	0.643	0.666	0.625	0.588	0.570	−0.063	−0.058	−0.055	91.4	92.0	92.6
July 2006												
0.04°	0.370	0.431	0.445	1.066	1.036	1.028	−0.055	−0.051	−0.052	92.1	92.3	93.0
0.24°	0.453	0.534	0.558	0.837	0.796	0.783	−0.055	−0.051	−0.052	91.5	91.7	92.5
0.48°	0.506	0.597	0.626	0.704	0.660	0.645	−0.055	−0.051	−0.052	91.0	91.4	92.2
1.00°	0.569	0.668	0.697	0.554	0.510	0.495	−0.055	−0.051	−0.052	90.5	91.0	91.8
August 2006												
0.04°	0.400	0.434	0.449	1.042	1.021	1.015	−0.059	−0.056	−0.055	92.0	92.3	92.7
0.24°	0.493	0.541	0.564	0.812	0.781	0.770	−0.059	−0.056	−0.055	91.1	91.5	92.0
0.48°	0.557	0.610	0.636	0.678	0.642	0.629	−0.059	−0.056	−0.055	90.6	91.1	91.6
1.00°	0.637	0.688	0.715	0.519	0.485	0.471	−0.059	−0.055	−0.055	90.0	90.7	91.1
February 2007												
0.04°	0.324	0.365	0.393	0.509	0.501	0.495	−0.009	−0.009	−0.006	91.8	92.0	92.0
0.24°	0.376	0.423	0.455	0.462	0.452	0.443	−0.012	−0.012	−0.009	91.8	92.0	92.3
0.48°	0.413	0.461	0.495	0.426	0.414	0.406	−0.013	−0.013	−0.010	92.5	91.8	92.1
1.00°	0.466	0.513	0.546	0.368	0.357	0.349	−0.014	−0.014	−0.011	91.0	91.4	91.9
March 2007												
0.04°	0.410	0.453	0.479	0.606	0.604	0.594	−0.013	−0.013	−0.011	92.1	92.4	92.6
0.24°	0.466	0.515	0.548	0.550	0.533	0.520	−0.015	−0.015	−0.013	92.0	92.3	92.7
0.48°	0.509	0.560	0.596	0.493	0.475	0.460	−0.016	−0.016	−0.014	91.7	92.0	92.6
1.00°	0.575	0.627	0.665	0.405	0.386	0.370	−0.017	−0.016	−0.015	91.4	91.9	92.5

datasets, containing IR pixel brightness temperatures and interpolated MW rainfall estimates, are compiled for a circular neighborhood surrounding the given pixel location. The IR data are sorted into descending order and the MW rainfall data are independently sorted into ascending order. The rank of the center IR pixel within the sorted dataset is then determined and used to select the rainfall value with the same rank from the independently sorted MW data. Applying this procedure at every pixel location creates a rainfall field in which rainfall maxima have been moved to local IR minima. The collocation procedure is, of course, imperfect and will introduce a degree of additional uncertainty into the MW rainfall estimates over and above the original rainfall measurement error. In addition, the collocated fields display a spatial variability commensurate with the original MW sensor resolutions rather than the GEO pixel resolution at which they are generated. These uncertainties are taken into account by the updating procedures.

3. Results

The LMODEL algorithm generates three sets of precipitation products corresponding to three stages of the technique: stage 1 products are outputs from the unadjusted model; stage 2 products use the interpolated process scaling parameter; and stage 3 products incorporate both rainfall-process scaling and Kalman filter state adjustment. The stage 1 products were generated using two seasonal calibrations—July–August 2006 and February–March 2007—from MW data (Bellerby et al. 2009). The LMODEL rainfall products were initially generated at a 0.04° spatial resolution and 30-min temporal resolution and then aggregated to create coarser-resolution products.

Table 1 details a validation of 3-h LMODEL rainfall products against ground radar at a range of spatial resolutions. From stage 1 to stage 3, the table shows a progressive improvement for all statistics: correlation coefficient, root-mean-square error (RMSE), bias, and skill score. The Kalman filter–adjusted (stage 3) products perform significantly better than the stage 1 and stage 2 products in both summer and winter at all product resolutions, demonstrating the effectiveness of the Kalman filter data-adjustment strategy and suggesting that this updating stage is relatively robust with respect to the choice of error model. Table 1 also shows some variations in algorithm performance with season. Products from all three stages show higher correlations in the summer months (June–August), whereas lower RMSE and bias values were found in the winter period (February and March). The skill scores are similar for all seasons,

TABLE 3. Validation of 3-h LMODEL stage 3 outputs against ground radar data compared to a validation of 3-h MW data against ground radar data. The latter validation was only performed for grid cells where at least one MW overpass was available in the 3-h interval and at least 50% of the measurement cell was covered by all available overpasses.

Resolution	Correlation (r)		RMSE (mm h^{-1})		Bias (mm h^{-1})		Skill (%)	
	LMODEL	MW	LMODEL	MW	LMODEL	MW	LMODEL	MW
June 2006 (MW 97% coverage)								
0.04°	0.544	0.473	0.840	0.983	−0.55	−0.034	92.8	94.0
0.24°	0.618	0.552	0.714	0.813	−0.55	−0.034	92.9	93.5
0.48°	0.660	0.605	0.633	0.697	−0.55	−0.034	92.8	93.1
1.00°	0.714	0.666	0.511	0.541	−0.55	−0.034	92.7	92.6
July 2006 (MW 94% coverage)								
0.04°	0.543	0.494	0.812	1.011	−0.051	−0.019	92.2	93.9
0.24°	0.643	0.595	0.637	0.792	−0.051	−0.018	92.2	93.3
0.48°	0.697	0.657	0.540	0.655	−0.050	−0.018	92.1	92.9
1.00°	0.753	0.723	0.433	0.495	−0.051	−0.018	92.1	92.5
August 2006 (MW 93% coverage)								
0.04°	0.546	0.503	0.797	1.002	−0.055	−0.023	92.0	93.2
0.24°	0.649	0.607	0.622	0.788	−0.055	−0.023	91.7	92.4
0.48°	0.707	0.667	0.522	0.655	−0.055	−0.023	91.6	92.1
1.00°	0.768	0.734	0.409	0.492	−0.054	−0.022	91.4	91.7
February 2007 (MW 75% coverage)								
0.04°	0.461	0.410	0.420	0.509	−0.007	−0.012	92.7	93.9
0.24°	0.511	0.477	0.386	0.446	−0.010	−0.013	92.0	93.5
0.48°	0.542	0.525	0.360	0.399	−0.011	−0.014	92.0	93.3
1.00°	0.584	0.587	0.317	0.330	−0.012	−0.015	91.8	93.4
March 2007 (MW 92% coverage)								
0.04°	0.561	0.488	0.481	0.720	−0.011	−0.012	92.2	94.2
0.24°	0.645	0.545	0.431	0.635	−0.013	−0.012	92.5	93.9
0.48°	0.651	0.558	0.391	0.560	−0.014	−0.013	92.5	93.7
1.00°	0.703	0.663	0.327	0.441	−0.015	−0.013	92.6	93.7

ranging from 90% to 92%. These results suggest that the LMODEL performs most effectively in the summer, when convective storms dominate, resulting in favorable correlation coefficients. In the winter period, stratiform rain is more prevalent, with lower rainfall intensities resulting in lower RMSE values; however, difficulties in identifying stratiform cloud development processes result in lower correlation coefficients. The lower correlations in the winter period may also be related to the quality of MW rainfall, which is much less accurate (or not available) in the presence of frozen surfaces and snowfall.

Table 2 shows the validation of 1-h LMODEL rainfall products against ground radar at a range of spatial resolutions. The results are consistent with the 3-h product evaluation described in Table 1, with stage 3 products consistently yielding the best validation statistics. These statistics further confirm that the Kalman filter–adjusted LMODEL is both stable and effective across different spatial and temporal scales. The very promising error statistics—particularly at 0.5° and 1° spatial resolutions—suggest that LMODEL rainfall estimates may be useful at the fine time scales needed for hydrological applications.

Table 3 compares validation statistics for 3-h LMODEL stage 3 outputs against ground radar data to equivalent validation statistics for a MW-only rainfall product. The latter validation was only performed for grid cells where at least one MW overpass was available in the 3-h interval and at least 50% of the measurement cell was covered by the overlapping areas of all available overpasses. The improved sampling capability provided by constellation LEO satellites, culminating in GPM, should guarantee at least one MW rainfall sample within every 3-h period. However, as discussed earlier, using 3-h instantaneous samples may cause both over- and undercatch of 3-h average rainfall. Although current MW sensor availability does not guarantee a 3-h return period, the MW test dataset provides this for ∼90% of the available points (more if the definition of a valid sample is relaxed). This comparison shows that the performance of LMODEL is consistently better than that of MW estimates for both summer and winter in terms of both correlation coefficients and RMSE. This implies that LMODEL, by employing an effective integration of LEO and GEO satellite information, provides added value over a 3-h rainfall product using LEO satellite MW rainfall data alone.

Figure 2 plots correlations against radar for 3-h LMODEL stage 3 and MW data. Within each 3-h period, an average rainfall within each 0.24° grid box was calculated from the available samples from each data
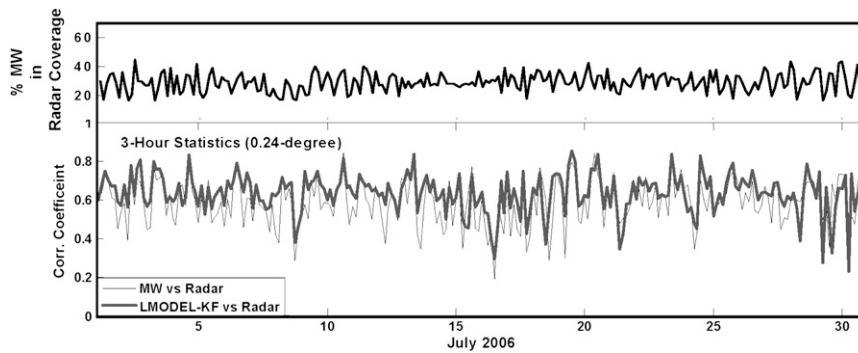
FIG. 2. Correlations for 0.25° 3-h LMODEL stage 3 rainfall against ground radar data plotted against time for July 2006 and compared with corresponding correlations for MW rainfall against ground radar. The percentage coverage of MW rainfall data over total radar coverage is also shown.

source (radar, LMODEL, or MW), and the resulting coincident 3-h rainfall data were used to calculate the corresponding correlation coefficients. This contrasts with Table 3, where more stringent data-availability criteria were applied. Correlation coefficients range from 0.13 to 0.76 for the radar–MW comparison and from 0.20 to 0.85 for radar–LMODEL stage 3 comparison. Although the range of correlations is similar for both sets of 3-h products, the LMODEL rainfall yields much higher correlations than MW rainfall when the correlations for the latter fall below 0.6. In addition, the correlations for MW rainfall vary abruptly between low and high values, indicating that these estimates perform less consistently throughout the evaluation period. Overall, LMODEL outperforms MW with mean 3-h correlations of 0.634 and 0.588, respectively. This result is consistent with the overall dataset correlations presented in Table 3. Figure 3 replicates Fig. 2 for August 2006. Again, correlation coefficients range from 0.10 to 0.76 for the radar–MW comparison and from 0.16 to 0.79 for the radar–LMODEL stage 3 comparison. Overall, LMODEL outperforms the MW-only product with mean 3-h correlations of 0.644 and 0.597, respectively.

Figure 4 shows scatterplots of 3-h LMODEL stage 3 and MW rainfall against radar and additionally compares LMODEL–radar correlations to the fractional coverage of MW samples. Data points for both plots were computed for each 3-h time step in August 2006. The percentage of MW samples was based on the ratio of available 30-min 0.04° MW rainfall samples to the maximum number of 30-min 0.04° samples that could occur under the radar coverage. Figure 4a shows a strong correlation between LMODEL–radar and MW–radar correlations. LMODEL outputs consistently outperform the MW-only product, with the majority of samples laying above the 1:1 line, and significant improvements are apparent for samples with low MW–radar correlations. Figure 4b shows LMODEL–radar correlations varying across a broad range for samples with low MW availability and adopting consistently high values for samples benefiting from significant MW availability—although this relationship between correlations and coverage is extremely weak.

Figures 5 and 6 show example 3-h LMODEL stage 2 rainfall maps for two different times. In the summer example shown in Fig. 5, both MW and LMODEL stage 3
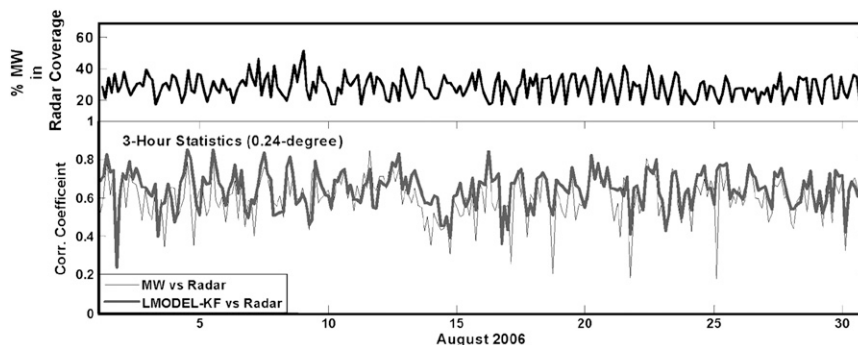

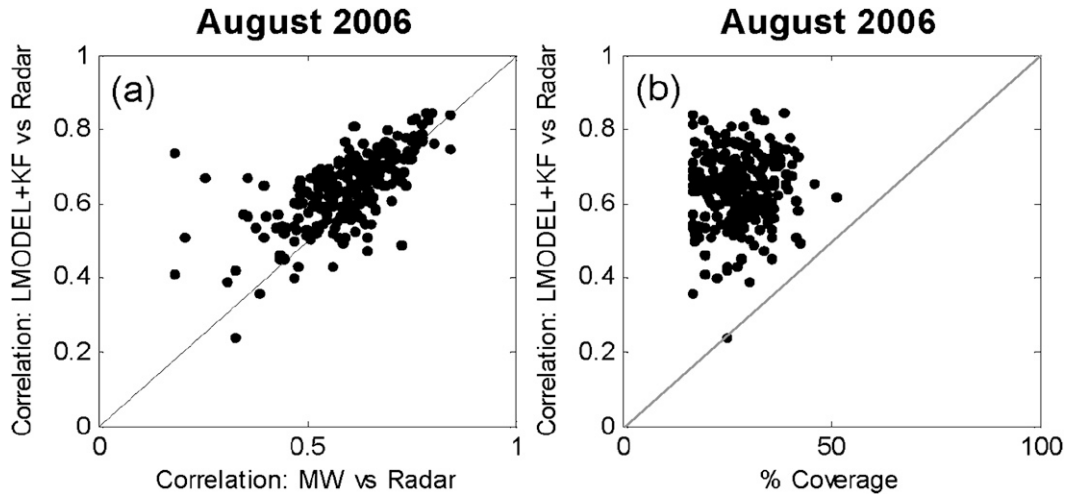FIG. 3. Same as Fig. 2 but for August 2006.

FIG. 4. (a) Scatterplot for August 2006 of correlation of 3-h LMODEL stage 3 rainfall to radar rainfall vs the correlation of 3-h MW rainfall to radar rainfall. (b) Same as for (a) but versus fractional (%) MW coverage (computed at full GEO pixel resolution).

capture heavy rainfall over southeastern Arizona, northeastern Texas, and southern Kansas and Missouri while underestimating rain areas over Indiana compared to the radar. In addition, MW overestimates rainfall over southern Arizona and Kansas. In the winter example shown in Fig. 6, both MW and LMODEL stage 3 capture heavy rainfall over western Oklahoma, whereas

the 3-h MW rainfall seems to overestimate rainfall in southern Arizona but miss rainfall over Illinois and Iowa. The MW data do not cover New York and New England, most likely because of problems with a snow-covered surface. However, the LMODEL stage 3 estimates effectively capture the rainfall over the MW data void but overestimate the rain area in southern Arizona
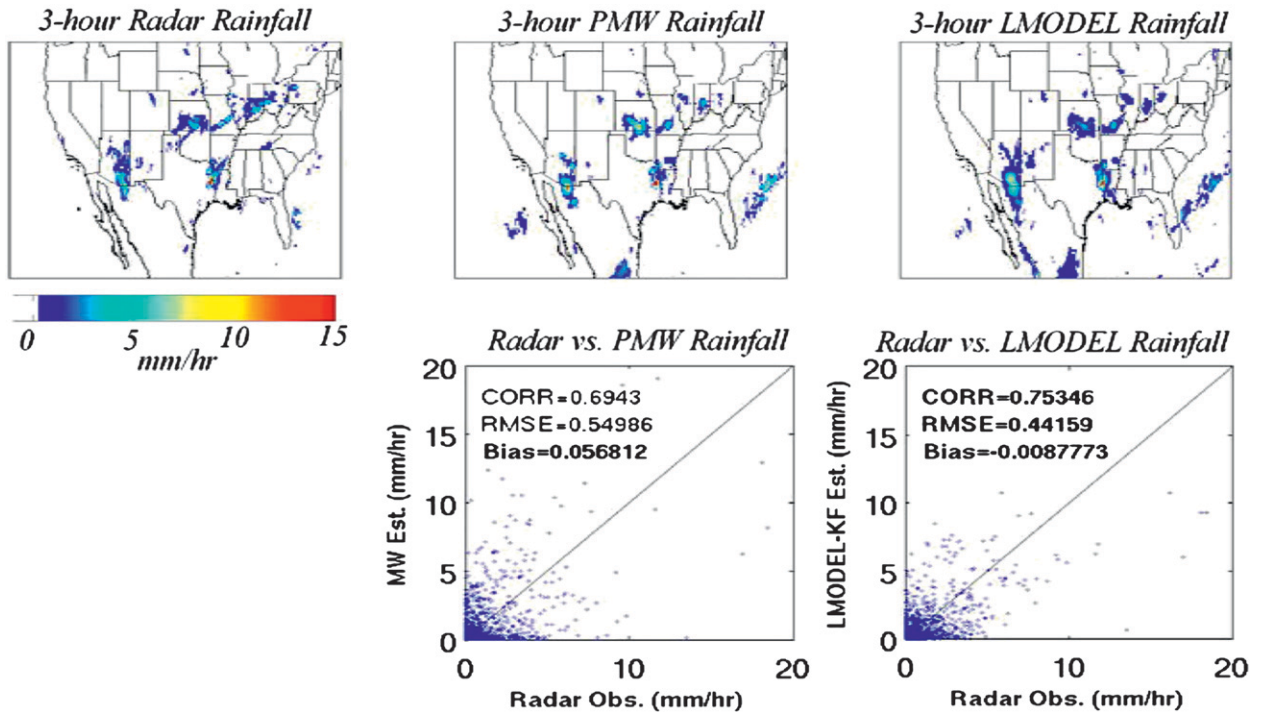
FIG. 5. Maps for 3-h 0.24° resolution, radar, MW, and LMODEL (stage 3) rainfall for 0900–1200 UTC 27 Jul 2006, together with corresponding scatterplots of LMODEL and MW rainfall against ground radar.
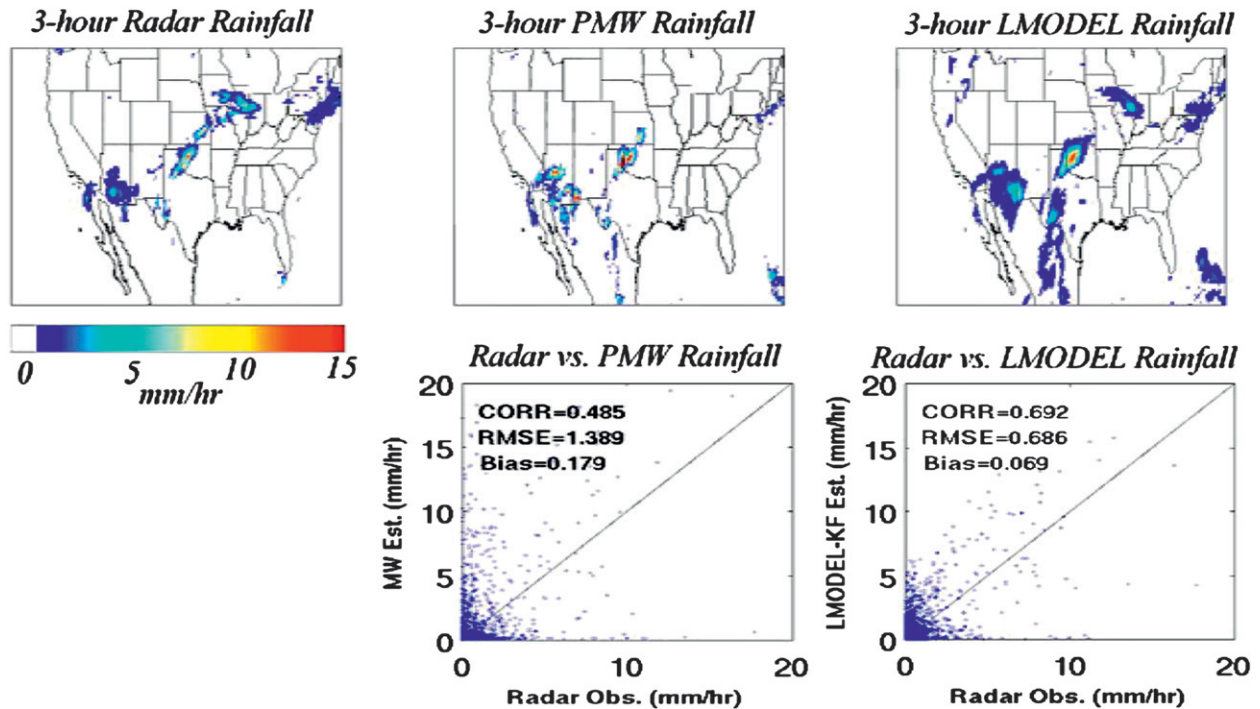
FIG. 6. Same as Fig. 5 but for 0000–0300 UTC 23 Mar 2006.

and west Texas. The scatterplots for both examples show LMODEL stage 3 performing better than MW estimates, as characterized by the validation statistics tabulated over the plots.

Figure 7a plots product–observation correlations against time from the nearest MW overpass for three rainfall products: 1) unadjusted 0.04° LMODEL outputs (stage 1); 2) LMODEL outputs adjusted using local calibration and the Kalman filter (stage 3); and 3) a simple linear interpolation of collocated MW rainfall along advection streamlines. The validation dataset for this comparison was formed by removing every 10th MW overpass from the calibration dataset and rerunning the LMODEL and rainfall-advection products for July–August 2006 with these overpasses removed. Validation was then performed against the collocated MW data that had been held back. The LMODEL stage 1 products show a correlation of ~0.6 to the MW reference data, which is, of course, independent of time from the nearest MW overpass. The dashed line shows the decay in correlation for the MW advection product with time from the nearest overpass. Correlations drop significantly from 1.0 to 0.6 after 30 min and further decay to ~0.4 only an hour from the nearest MW measurement. This implies that there is a limitation to the direct use of high-resolution advection vectors to morph MW rainfall between overpasses, with an effective "window" of less than one hour beyond which the accuracy of

advected rainfall fields diminishes significantly. Notice that the standard CMORPH algorithm operates at a very different spatial resolution to the MW advection product assessed here, so this result is not transferable to that algorithm. The LMODEL stage 3 products, on the other hand, behave very differently, displaying an impressively high correlation near 0.9 that remains stable up to three hours from the nearest overpass. However, it must be noted that this comparison is made against the collocated MW product, which by its nature introduces aspects of the IR cloud geometry into its corrected rainfall field.

Figure 7b shows the fractional occurrence of time from the nearest MW overpass computed for 0.04° GEO pixels in the test dataset for July–August 2006. About 80% of the samples are in the range of within one hour from the nearest MW overpass, whereas nearly 15% of the samples are 1–2 h from a MW overpass. Around 5% of the samples lie in the range of 2–3 h from the nearest MW overpass.

Table 4 compares validation statistics against independent MW for the linearly interpolated morphing product and LMODEL stages 1 and 3. These statistics were computed only for points for which a MW measurement was not available. The high-resolution morphing technique demonstrates the poorest performance, followed by LMODEL stage 1 and LMODEL stage 2. Again, this indicates the strength of LMODEL at
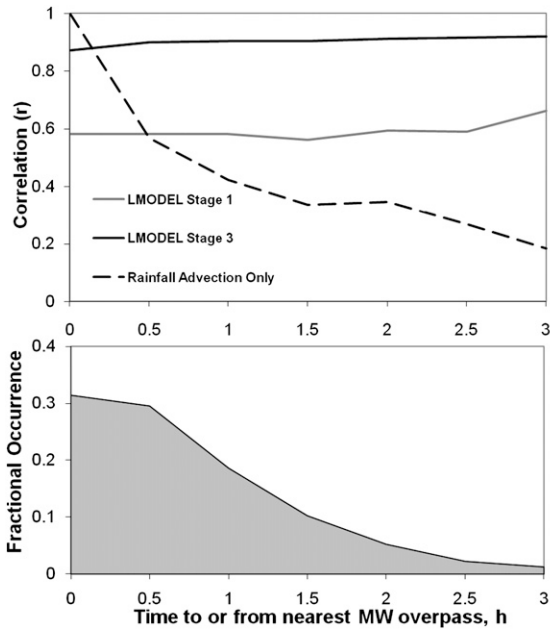
FIG. 7. (a) Product correlation against independent collocated MW data plotted against time from the nearest incorporated MW overpass for three 0.04° 30-min rainfall products covering July–August 2006: LMODEL stage 1, LMODEL stage 3, and a simple linear interpolation of collocated MW rainfall along advection streamlines. (b) Fractional occurrence of time from nearest MW overpass computed for 0.04° GEO pixels in the test dataset for July–August 2006.

reproducing microwave rainfall fields at high resolution. The result does not, however, constitute a cross validation against the standard CMORPH algorithm, which uses a lower resolution and empirically corrected representation of cloud advection (Joyce et al. 2004).

Figure 8 compares rainfall propagation speeds found in LMODEL stage 1 outputs and ground radar data using time–longitude diagrams. As discussed earlier, Joyce et al. (2004) notice a significant systematic difference (ratio of ~2–4) between cloud advection speeds and rainfall advection, attributable to cirriform clouds shearing off from precipitating systems. However, it is clear that some GEO satellite features such as overshooting tops will move with surface rainfall, even if they

are spatially displaced from corresponding features at ground level (Adler and Mack 1986; Adler and Negri 1988). GEO satellite forcing in LMODEL concentrates on growing clouds, whereas the cloud advection is determined at near-pixel resolutions. These two factors should combine to make the model relatively robust with respect to the decoupling of cloud and rainfall motion; however, being based on single-band IR imagery, LMODEL is not immune to problems associated with cirrus contamination. Although some differences in feature delineation are apparent in Fig. 8, observed and modeled propagation speeds match each other reasonably well, and there is no apparent need for a significant systematic correction of advection velocities, as is applied in CMORPH.

4. Conclusions

This paper presents a 5-month case study covering the continental United States to validate the new LMODEL satellite rainfall algorithm. The algorithm proceeds in three stages, and the validation statistics presented show a consistent improvement in LMODEL performance, from employing fixed seasonal parameter sets (stage 1) through the addition of time-interpolated precipitation-process scaling parameters (stage 2) to the implementation of model state updating using a Kalman filter (stage 3). A comparison of 3-h stage 3 LMODEL and MW rainfall estimates against ground radar rainfall shows that the LMODEL outputs outperform collocated 3-h MW rainfall in terms of evaluation statistics such as correlation and root-mean-square error. The performance of LMODEL stage 3 outputs remains quite stable between MW overpasses (see Fig. 7). The correlation coefficient for 0.04° LMODEL outputs against cloud-corrected MW data stays relatively constant at around 0.9 more than 3-h from the nearest MW overpass. By comparison, equivalent correlations for a high-resolution morphing product (in which rainfall rates are linearly interpolated along advection streamlines) drop from 1.0 to around 0.4 as time from the nearest overpass increases from zero to three hours. Validation statistics comparing LMODEL to

TABLE 4. Validation against independent MW data of 30-min 0.04° LMODEL stage 1 and stage 3 outputs and a simple linear interpolation of collocated MW rainfall along advection streamlines (morph).

Correlation (r)			RMSE (mm h^{-1})		
Morph	LMODEL stage 1	LMODEL stage 3	Morph	LMODEL stage 1	LMODEL stage 3
0.431	0.579	0.906	0.930	0.723	0.441
Bias (mm h^{-1})			Skill (%)		
Morph	LMODEL stage 1	LMODEL stage 3	Morph	LMODEL stage 1	LMODEL stage 3
0.017	−0.078	−0.081	66.6%	74.4%	75.5%

July 2006, Latitude 38°N

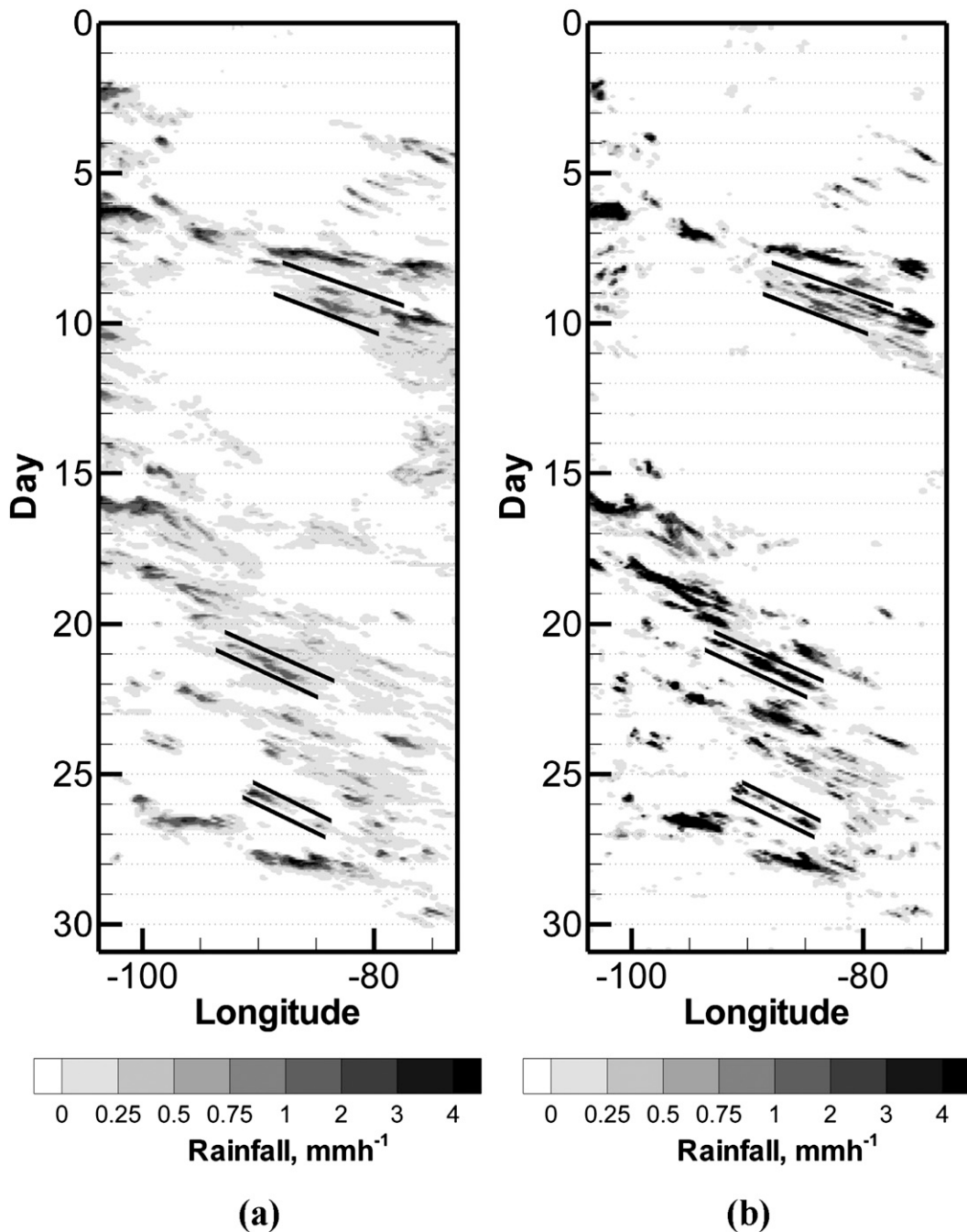

FIG. 8. Time–longitude diagrams for (a) hourly 0.24° LMODEL stage 1 rainfall outputs and (b) hourly ground radar rainfall measurements aggregated to the same spatial resolution.

the high-resolution morphing product confirm the superior performance of LMODEL at representing rainfall variability between MW overpasses. Moreover, an analysis of rainfall motion suggests that LMODEL is capable of relating rainfall advection to cloud advection without

the need for an empirical correction to advection velocities. High-temporal-resolution validation statistics for LMODEL stage 3 products are very encouraging and suggest that LMODEL has the potential to generate effective rainfall measurements at an hourly scale. It should

be noted, however, that LMODEL has not yet been cross validated against operational rainfall products such as CMORPH. Such an intercomparison is a priority for further research.

The LMODEL algorithm is not fully real time; that is, a full stage 2 correction can only take place up to the last available microwave overpass. However, the algorithm is able to generate estimates right up to the present. These estimates must use a constant value for the precipitable water scaling parameter determined in stage 2 rather than interpolated values. However, in all other respects they will be identical to other LMODEL stage 3 outputs and thus the algorithm has some potential for real-time applications, such as flash-flood forecasting.

This study has demonstrated the potential for generating improved rainfall estimates using a combined cloud tracking/cloud modeling/model updating scheme. The individual components of this scheme have been deliberately kept as simple as possible and all are amenable to improvement. Currently, cloud growth processes are characterized using only one GEO channel (thermal IR) with local cloud-top brightness temperatures and their temporal gradient the sole determinants of precipitable water input to storm systems. Future work will explore using multispectral GEO imagery to better characterize rainfall processes. In addition, improved model parameterizations will be investigated, with a view toward developing regional and global parameterizations for operational LMODEL implementation.

REFERENCES

Adams, D. K., and A. C. Comrie, 1997: The North American monsoon. *Bull. Amer. Meteor. Soc.,* **78,** 2197–2213.

Adler, R. F., and R. A. Mack, 1986: Thunderstorm cloud top dynamics as inferred from satellite observations and a cloud top parcel model. *J. Atmos. Sci.,* **43,** 1945–1960.

——, and A. J. Negri, 1988: A satellite infrared technique to estimate tropical convective and stratiform rainfall. *J. Appl. Meteor.,* **27,** 30–38.

Arkin, P. A., and B. N. Meisner, 1987: The relationship between large-scale convective rainfall and cold cloud over the Western Hemisphere during 1982–84. *Mon. Wea. Rev.,* **115,** 51–74.

Ashley, W. S., T. L. Mote, P. G. Dixon, S. L. Trotter, E. J. Powell, J. D. Durkee, and A. J. Grundstein, 2003: Distribution of mesoscale convective complex rainfall in the United States. *Mon. Wea. Rev.,* **131,** 3003–3017.

Ba, M. B., and A. Gruber, 2001: GOES Multispectral Rainfall Algorithm (GMSRA). *J. Appl. Meteor.,* **40,** 1500–1514.

Bellerby, T., 2004: A feature-based approach to satellite precipitation monitoring using geostationary IR imagery. *J. Hydrometeor.,* **5,** 910–921.

——, 2006: High-resolution 2-D cloud-top advection from geostationary satellite imagery. *IEEE Trans. Geosci. Remote Sens.,* **44,** 3639–3648.

——, M. Todd, D. Kniveton, and C. Kidd, 2000: Rainfall estimation from a combination of TRMM precipitation radar and GOES multispectral satellite imagery through the use of an artificial neural network. *J. Appl. Meteor.,* **39,** 2115–2128.

——, K. Hsu, and S. Sorooshian, 2009: LMODEL: A satellite precipitation methodology using cloud development modeling. Part I: Algorithm construction and calibration. *J. Hydrometeor.,* **10,** 1081–1095.

Capacci, D., and B. J. Conway, 2005: Delineation of precipitation areas from MODIS visible and infrared imagery with artificial neural networks. *Meteor. Appl.,* **12,** 291–305.

Court, A., 1974: The climate of the conterminus United States. *Climates of North America,* R. A. Bryson and F. K. Hare, Eds., Vol. 11, *World Survey of Climatology,* Elsevier, 193–261.

CPC, cited 2008: NOAA CPC merged microwave. [Available online at http://www.cpc.ncep.noaa.gov/products/janowiak/mwcomb_description.html.]

Ferraro, R. R., F. Weng, N. C. Grody, and L. Zhao, 2000: Precipitation characteristics over land from the NOAA-15 AMSU sensor. *Geophys. Res. Lett.,* **27,** 2669–2672.

Hong, Y., K. Hsu, S. Sorooshian, and X. Gao, 2004: Precipitation estimation from remotely sensed imagery using an artificial neural network cloud classification system. *J. Appl. Meteor.,* **43,** 1834–1852.

Horsfield, N., 2006: Development of a mass balance approach to modelling cloud lifecycles and rainfall using satellite observations. Ph.D. thesis, University of Hull, 353 pp.

Hou, A., G. S. Jackson, C. Kummerow, and J. M. Shepherd, 2008: Global precipitation measurement. *Precipitation: Advances in Measurement, Estimation, and Prediction,* S. Michaelides, Ed., Springer, 131–170.

Hsu, K., X. Gao, S. Sorooshian, and H. V. Gupta, 1997: Precipitation estimation from remotely sensed information using artificial neural networks. *J. Appl. Meteor.,* **36,** 1176–1190.

Huffman, G. J., and Coauthors, 2007: The TRMM Multisatellite Precipitation Analysis (TMPA): Quasi-global, multiyear, combined-sensor precipitation estimates at fine scales. *J. Hydrometeor.,* **8,** 38–55.

ISDR, 2008: Early warning systems can save lives when cyclones strike. Press Release UN/ISDR 2008/05, 1 pp. [Available online at http://www.unisdr.org/eng/media-room/press-release/2008/pr-2008-06-myanmar-cyclone-nargis.pdf.]

Janowiak, J. E., R. J. Joyce, and Y. Yarosh, 2001: A real-time global half-hourly pixel-resolution infrared dataset and its applications. *Bull. Amer. Meteor. Soc.,* **82,** 205–217.

Joyce, R. J., J. E. Janowiak, P. A. Arkin, and P. Xie, 2004: CMORPH: A method that produces global precipitation estimates from passive microwave and infrared data at high spatial and temporal resolution. *J. Hydrometeor.,* **5,** 487–503.

Kidd, C., D. R. Kniveton, M. C. Todd, and T. J. Bellerby, 2003: Satellite rainfall estimation using combined passive microwave and infrared algorithms. *J. Hydrometeor.,* **4,** 1088–1104.

Kummerow, C., W. Barnes, T. Kozu, J. Shiue, and J. Simpson, 1998: The Tropical Rainfall Measuring Mission (TRMM) sensor package. *J. Atmos. Oceanic Technol.,* **15,** 809–817.

——, and Coauthors, 2000: The status of the Tropical Rainfall Measuring Mission (TRMM) after two years in orbit. *J. Appl. Meteor.,* **39,** 1965–1982.

——, and Coauthors, 2001: Evolution of the Goddard profiling algorithm (GPROF) for rainfall estimation from passive microwave sensors. *J. Appl. Meteor.,* **40,** 1801–1820.

Lin, Y., and K. E. Mitchell, 2005: The NCEP stage II/IV precipitation analyses: Development and applications. Preprints, *19th Conf. on Hydrology,* San Diego, CA, Amer. Meteor. Soc., 1.2. [Available online at http://ams.confex.com/ams/Annual2005/techprogram/paper_83847.htm.]

Machado, L. A. T., W. B. Rossow, R. L. Guedes, and A. W. Walker, 1998: Life cycle variations of mesoscale convective systems over the Americas. *Mon. Wea. Rev.,* **126,** 1630–1654.

Martine, G., and A. Marshall, 2007: *UNFPA State of World Population, 2007: Unleashing the Potential of Urban Growth.* United Nations Population Fund, 108 pp.

Marzano, F. S., M. Palmacci, D. Cimini, G. Giuliani, and F. J. Turk, 2004: Multivariate statistical integration of satellite infrared and microwave radiometric measurements for rainfall retrieval at the geostationary scale. *IEEE Trans. Geosci. Remote Sens.,* **42,** 1018–1032.

Nicholson, S. E., and Coauthors, 2003a: Validation of TRMM and other rainfall estimates with a high-density gauge dataset for West Africa. Part I: Validation of GPCC rainfall product and pre-TRMM satellite and blended products. *J. Appl. Meteor.,* **42,** 1337–1354.

——, and Coauthors, 2003b: Validation of TRMM and other rainfall estimates with a high-density gauge dataset for West Africa. Part II: Validation of TRMM rainfall products. *J. Appl. Meteor.,* **42,** 1355–1368.

Okamoto, K., T. Iguchi, N. Takahashi, K. Iwanami, and T. Ushio, 2005: The Global Satellite Mapping of Precipitation (GSMaP) project. *Proc. Int. Geoscience and Remote Sensing Symp.,* Seoul, South Korea, Institute of Electrical and Electronics Engineers, 3414–3416.

Simpson, J., R. F. Adler, and G. R. North, 1988: A proposed Tropical Rainfall Measurement Mission (TRMM) satellite. *Bull. Amer. Meteor. Soc.,* **69,** 278–295.

Solomon, S., D. Qin, M. Manning, M. Marquis, K. Averyt, M. M. B. Tignor, H. L. Miller Jr., and Z. Chen, 2007: *Climate Change 2007: The Physical Science Basis.* Cambridge University Press, 996 pp.

Sorooshian, S., K. Hsu, X. Gao, H. V. Gupta, B. Imam, and D. Braithwaite, 2000: Evaluation of PERSIANN system satellite-based estimates of tropical rainfall. *Bull. Amer. Meteor. Soc.,* **81,** 2035–2046.

Todd, M., C. Kidd, D. R. Kniveton, and T. J. Bellerby, 2001: A combined satellite infrared and passive microwave technique for estimation of small-scale rainfall. *J. Atmos. Oceanic Technol.,* **18,** 742–755.

Turk, F. J., and S. D. Miller, 2005: Toward improving estimates of remotely-sensed precipitation with MODIS/AMSR-E blended data techniques. *IEEE Trans. Geosci. Remote Sens.,* **43,** 1059–1069.

Vicente, G., R. A. Scofield, and W. P. Mensel, 1998: The operational GOES infrared rainfall estimation technique. *Bull. Amer. Meteor. Soc.,* **79,** 1881–1898.

Weng, F., L. Zhao, R. Ferraro, G. Pre, X. Li, and N. C. Grody, 2003: Advanced microwave sounding unit cloud and precipitation algorithms. *Radio Sci.,* **38,** 8068, doi:10.1029/2002RS002679.

Xu, L., X. Gao, S. Sorooshian, P. A. Arkin, and B. Imam, 1999: A microwave infrared threshold technique to improve the GOES precipitation index. *J. Appl. Meteor.,* **38,** 569–579.